

RESEARCH

Open Access



Time-Dependent Analysis of Precast Segmental Bridges

Gian Felice Giaccu¹, Davide Solinas¹, Bruno Briseghella^{2*}  and Luigi Fenu³

Abstract

Prestressed segmentally constructed balanced cantilever bridges are often subjected to larger deflections than those predicted by calculations, especially for long-term effects. In this paper, the case of modular balanced cantilever bridges, which are prestressed segmental bridges obtained through a repetition of the same double cantilever, is investigated. The considered bridges are two typical cases of modular balanced cantilever both subjected to large deformations during their lifetime. In this case, due to the unusual employed static scheme, creep deflections indefinitely evolve over time particularly at the end of the cantilevers and in correspondence with the central joint. These remarkable deflections cause discomfort for vehicular traffic and in certain cases can lead to the bridge collapse. Important extraordinary maintenance interventions were necessary to restore the viability of the bridges and to replace the viaduct design configuration. To this aim, the static schemes of the structures were varied, introducing new constraints, new tendons, and carbon fiber reinforcements. In the present work, time analysis was performed to compare the time-dependent behavior of the bridge according to two different creep models, the CEB-FIP Model Code 2010 and the RILEM Model B3, with the real-time-dependent behavior of the bridge observed during its lifetime. The two different employed models exhibit different behaviors in terms of displacements and bending moments acting on the bridge. Interesting considerations are made on their reliability in simulating the long-term creep effects that evolve indefinitely over time. Moreover, retrofitting techniques have been proposed and modeled to predict their effectiveness in reducing time-dependent deflections.

Keywords: span-by-span construction, precast segmental bridge, creep, shrinkage, vertical deflection, retrofitting

1 Introduction

Prestressed concrete segmental bridges are often subjected to considerable stress during launch. In these particular conditions, the actual displacements can be higher, especially for long-term deflections, than those predicted by simple finite element (FE) models usually employed by practitioners (Malm and Sundquist 2010; Pimanmas 2007); displacements may increase during the entire life of the structure, leading to significant inconvenience to traffic and to the structure (Bazant et al. 2008; Malm and Sundquist 2010). Moreover, long-term

deflections of prestressed bridges can be affected by various factors based on the thermo-hygro model behavior of cement, ambient temperature, humidity, and structural-specific surface area (Bazant and Baweja 1995; Maekawa et al. 2011). Recent works show how the final stage results of a segmentally constructed bridge are affected by the construction stages (Granata and Arici 2013; Granata et al. 2013; Vokunnaya et al. 2017). Large deflections on this typology of bridges can lead, in the absence of proper maintenance interventions, to the collapse of the structure (Neulichedl et al. 2008). The importance of investigating the long-term behavior of segmental cantilever bridges has been highlighted by Bazant and Hubler (2014): “Recent investigations prompted by a disaster in Palau revealed that worldwide, there are 69 long-span segmental prestressed-concrete box-girder bridges that

*Correspondence: bruno@fzu.edu.cn

² College of Civil Engineering, Fuzhou University, No. 2 Xue Yuan Road, Fuzhou 350108, Fujian, China

Full list of author information is available at the end of the article
Journal information: ISSN 1976-0485 / eISSN 2234-1315

suffered excessive multi-decade deflections, while many more surely exist.”

Noteworthy is the case of prestressed modular segmental bridges with symmetric span arrangement, having cantilever configuration in the end spans or in the proximity of the expansion joints. In these cases, especially for asymmetrical launch and for the excessive length of the end spans with respect to that of the inner spans, excessive long-term deflections can occur, causing significant discomfort to the vehicular traffic.

This is also the case for the “Navile” and “Sa Pruna” bridges, two precast segmental box girder bridges located on the east coast of Sardinia. Due to economic restrictions at the time, for the launching of both bridges, the employed construction technology included a single launching gantry. For both bridges, large deformations occurred shortly after their entry into service at the ends of the cantilevers, in correspondence with both abutments and in the middle point, where the joint is located (Giaccu et al. 2012).

The long-term behavior of these two bridges requested retrofitting interventions necessary to replace the serviceability limit state of the bridge, otherwise not compatible with its service conditions.

To investigate the time-dependent behavior of prestressed modular segmental bridges, an accurate FE model of the Navile Bridge has been developed, taking into account long-term creep, shrinkage and prestressing, aiming to accurately replicate the construction stages and ordinary and extraordinary maintenance interventions performed during the entire life of the bridge. Two different creep models, the CEB-FIP Model Code 2010 (2012) and the RILEM B3 model (Bazant and Baweja 1996), were utilized in comparison with real data, aiming to replicate a realistic structural behavior in terms of structural displacements.

The results of the FE modeling carried out using the two creep models have been also compared one another, because the two different models lead to different results, particularly in the case of long-term deformations.

Limits and advantages of applying the classical theory of bending when creep occurs in prestressed box girders, in particular of segmental bridges characterized by several construction stages (Malm and Sundquist 2010), have been investigated.

FE models with beam elements have been used to analyze how the unbalanced static schemes of the end span cantilevers, as well as of those of the central span, cause high long-term deflections at the lateral cantilever ends and at central mid-span. In fact, FE analyses have been carried out implementing the above two different creep models characterized by creep functions with significantly different long-term trends.

It has been evaluated which creep model is more suited to simulate the long-term behavior of prestressed modular segmental bridges and the beneficial effects with time of the retrofit interventions used in the analyzed case study.

2 Evolution of Material Properties

The structural response of segmentally constructed bridges is deeply affected by their material properties. It is fundamental to consider the evolution overtime of the material rheological properties, especially those of concrete and harmonic steel. While the latter are mainly subjected to relaxation, the former is subjected to creep, as well as to the evolution overtime of the elastic modulus and shrinkage deformations.

Creep deformations in concrete are generally nonlinearly related to stresses (Bažant et al. 1976); nevertheless, a linear correlation between stress and creep deformations can be postulated, assuming that the concrete stress is lower than 40% of the concrete compressive strength.

Linear creep models are implemented through defining the compliance (creep) function $J(t, t_0)$ representing the stress-dependent strain per unit stress, i.e., the response at time t to a sustained constant unit imposed stress applied at time t_0 (Levi and Pizzetti 1951). Compliance functions can be defined by theoretical models as Dischinger’s (Dischinger 1939) or Kelvin-Voigt’s ones (Voigt 1890). However, the compliance functions of modern linear creep models currently adopted in practice engineering are based on extrapolation of experimental data carried out over some decades in many laboratories all over the world.

Besides creep, also concrete relaxation affects the behavior in time of concrete segmental bridges, for their peculiar construction method. This means that the relaxation function $R(t, t_0)$ is to be defined, too. It represents the stress response at time t to a sustained constant unit imposed strain applied at time t_0 (Levi and Pizzetti 1951). Contrary to $J(t, t_0)$, $R(t, t_0)$ is hard to be empirically defined on the basis of experimental data. This is due to the difficulties in carrying out relaxation experiments, and therefore to the few experimental data available. Fortunately, using functional analysis, $R(t, t_0)$ can be obtained by $J(t, t_0)$ through numerical integration of the Volterra’s integral equation relating $R(t, t_0)$ to $J(t, t_0)$.

By defining the redistribution function $\xi(t, t_0, t_1)$, also related to $J(t, t_0)$ and $R(t, t_0)$, linear creep models can be extended also to the case of concrete structures whose static scheme is changed at time $t_1 > t_0$ (Levi and Pizzetti 1951), as stated by the third viscoelasticity theorem, originally valid only for the Dischinger’s creep kernel, and successively generalized by Chiorino for any creep function $J(t, t_0)$ (Chiorino et al. 1984).

This is actually the case of concrete segmental bridges, whose static scheme is continuously varying during the construction stages, while creep deformations evolve in the already constructed parts of the bridge (Chiorino and Lacidogna 1993; Chiorino et al. 1984). This is furthermore true for the modular cantilever bridges analyzed in this study, because their retrofitting needs the change of the static scheme of the end spans.

Therefore, for usual structural schemes and for regular bridge geometry, creep deflections can be reliably estimated using linear creep models (Bažant et al. 1976) for evaluating a proper camber during the construction stages (Malm and Sundquist 2010). In the present study, two linear creep models were implemented in the FE model of the Navile Bridge, namely, the linear creep model of the CEB-FIP Model Code 2010 (2012) and that of the RILEM Model B3 (Bazant and Baweja 1996). The latter is not the last published by RILEM, which, in 2015, published the RILEM Model B4 (Bazant 2015). Nevertheless, the reliability of creep deformations calculated using this updated model does not appear to be improved (Fanourakis 2017). For this reason, in this study, the RILEM Model B3 is used. The description of the creep models of the CEB-FIP MC 2010 and the RILEM Model B3, as well as their differences, are reported in the following.

The creep model of the CEB-FIP Model Code 2010 (2012) has been updated over some decades since 1964 with the CEB Recommendations for an International Code of Practice for Reinforced Concrete (1964), that included a section regarding creep. It was the result of the research conducted in Munich in the '50 s by Wagner (Wagner 1958, 1962) and Rüschi, that led Rüschi, Jungwirth, and Hilsdorf to the '70 s (Rüschi et al. 1973, 1983) to define the Improved Dischinger Method (IDM), an analytical solution of Volterra's integral equation. In IDM the aging viscoelastic model of Glanville-Whitney (Glanville 1933; Whitney 1932), characterized by a flow deformation only, was updated through adding a delayed elastic component. The IDM was finally included in the CEB-FIP Model Code 1972 (Chiorino et al. 1972), and widely used in structural engineering in the '70 s and '80 s. Munich group's research on creep was successively continued by Müller and Hilsdorf (Müller and Hilsdorf 1990), leading to the definition of the creep section of the CEB-FIP Model Code 1990 (1993), that is almost completely similar to that of the CEB-FIP Model Code 2010 (2012).

The RILEM creep model B3 (Bazant and Baweja 1996) derives from research carried out in the Northwestern University by Bazant's group since the '60 s (Bazant 1966). In 1972 Bazant (1972) proposed a simplified analytical model of the concrete creep function implemented in a numerical algorithm for solving Volterra's

equations. This work is on the basis of Bazant's successive research on creep, and therefore of the RILEM creep model B3 (Bazant and Baweja 1996). In fact, while improving the definition of the creep function $J(t, t_0)$, Bazant was aware that only numerical solutions of Volterra's equations can lead to reliable results in the evaluation of creep deformations. On one hand compliance, relaxation and redistribution functions of model B3 are in fact suited to be used in numerical solutions of Volterra's equations and implemented in FE models; on the other hand, among the other creep models, the RILEM model B3 stands out for being strongly founded on the complex physical and chemical laws governing the creep behavior of concrete (Bažant and Baweja 1995; Chiorino 2005). In model B3 the compliance function is the sum of three addends, instantaneous strain due to unit stress, compliance function for basic creep at constant moisture content (no moisture movement through the material), and drying creep (Bažant and Baweja 1995). Therefore, in the absence of moisture movements, only moisture changes due to cement hydration are accounted for by basic creep. Its formulation is based on the solidification theory, in which viscoelasticity is caused by solidification with interlinking of layers of a nonaging constituent, and it is assumed that the chemical constituents of cement paste are not aging (Carol and Bazant 1993). The additional creep caused by drying of B3 is peculiar and is due to a long-term drying process caused by environment exposure (Bazant and Xi 1994). Additional creep (drying creep) as well as shrinkage are therefore due to the related moisture movement that is described by solving the moisture diffusion equation (Bazant et al. 1987). The definition of the RILEM creep model B3 is based on the experimental data of a very large number of tests on concrete specimens and structures carried out in many decades all over the world and stored in the RILEM data bank (Bazant and Chern 1984; Bažant and Zebich 1983; Müller et al. 1999).

In Figs. 1 and 2 the utilized creep functions $J(t, t_0)$ of the CEB MC 2010 and of the RILEM model B3, respectively, are plotted in logarithmic time scale, for different instants t_0 and for fixed values of the parameters f_{ck} , RH and notional size h .

The different setting and definition of the above creep models leads to a clearly different response of their related creep functions. It is well described by their plot shown in Figs. 1 and 2, where, for time t tending to infinite, the creep function of the CEB-FIP Model Code tends to a horizontal asymptote, thus meaning that creep deformations tend to zero in the long term. The creep function of the RILEM model B3 tends instead to an oblique asymptote. This allows FE models implemented with the RILEM model B3 to capture even the long-term behavior

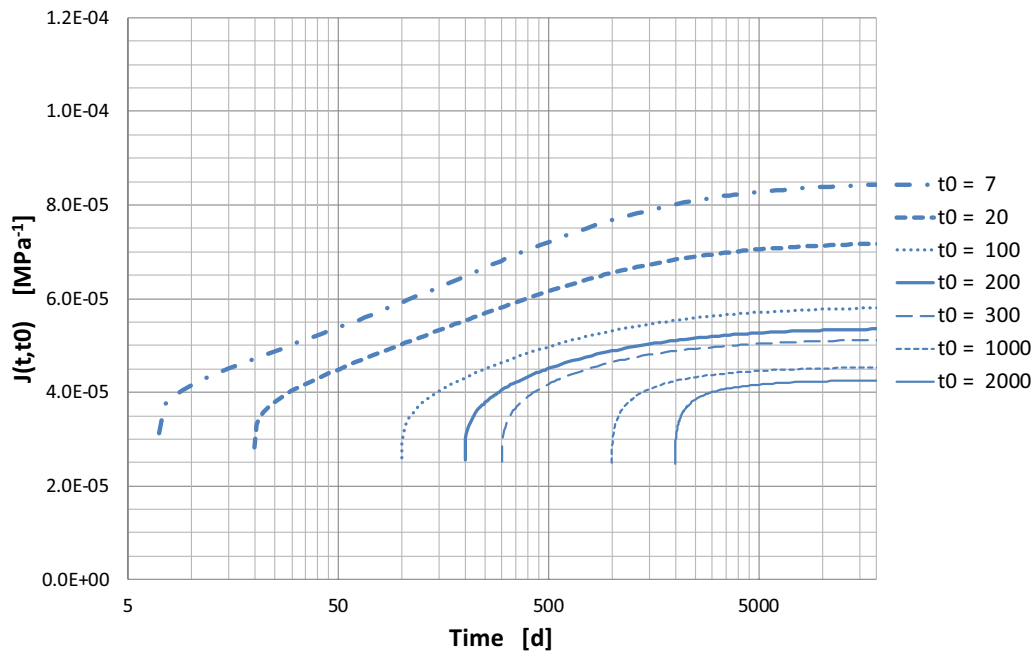


Fig. 1 Creep function $J(t, t_0)$ of the CEB MC 2010 for different instants t_0 with $f_{ck} = 40$ MPa, RH = 70% and $h = 330$ mm.

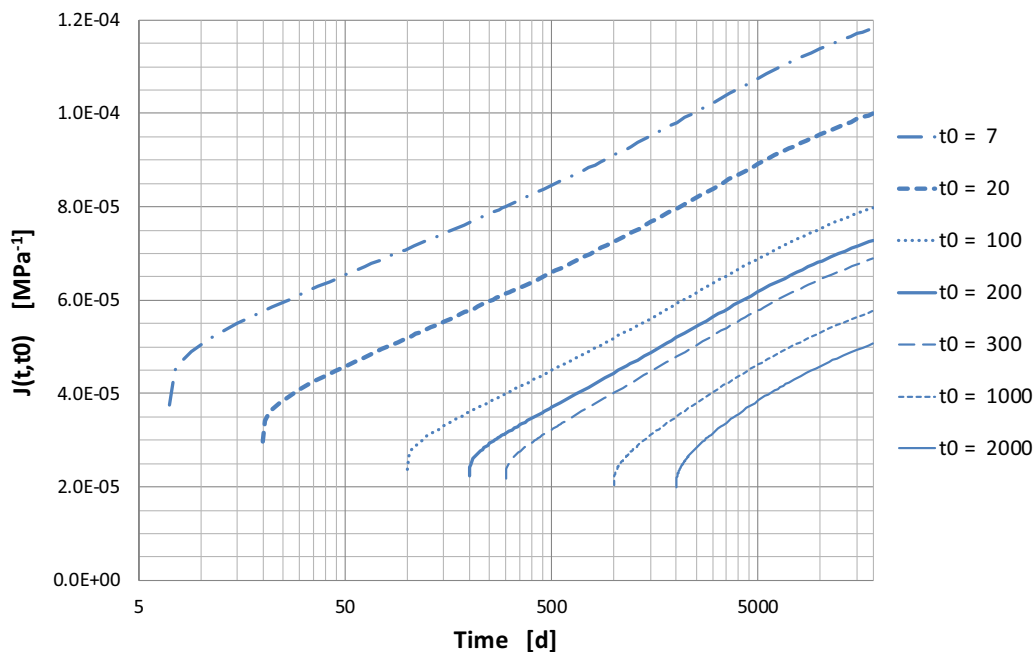


Fig. 2 Creep function $J(t, t_0)$ of the RILEM B3 model for different instants t_0 with $f_{ck} = 40$ MPa, RH = 70% and $h = 330$ mm.

of structures with deflections indefinitely evolving in time and internal forces indefinitely affected by imposed loads and/or deformations, and/or changes of the structural scheme at a certain time of the structure life cycle.

Sections 2.1 and 2.2 report the equations governing the two abovementioned creep models. Finally, relaxation of the prestressing tendons is taken into account according to Eurocode 2 (2004).

2.1 CEB-FIP Model Code 2010

2.1.1 Elastic Modulus

Elastic modulus depends on time, and the CEB-FIP Model Code 2010 by first referring to its value E_{ci} at 28 days:

$$E_{ci} = \alpha_E \left(\frac{f_{cm}}{f_{cm0}} \right)^{\frac{1}{3}} E_{c0}, \tag{1}$$

where f_{cm} is the average compressive strength of concrete at 28 days $f_{cm0} = 10$ (MPa), $E_{c0} = 2.15 \cdot 10^4$ (MPa), and α_E is a coefficient depending on aggregate type. Elastic modulus evolution over time is then valued as:

$$E_{ci}(t) = \sqrt{\beta_{cc}(t)} E_{ci} \tag{2}$$

with:

$$\beta_{cc}(t) = e^{s \left(1 - \sqrt{\frac{28}{t}} \right)}, \tag{3}$$

where t is the age of the concrete (expressed in days) and s is a coefficient depending on cement type.

2.1.2 Shrinkage

Regarding shrinkage, the Eurocode (2004) approach is used, where shrinkage is a summation of the autogenous shrinkage $\varepsilon_{ca}(t)$ and the drying shrinkage $\varepsilon_h(t)$.

The autogenous shrinkage develops at the earlier curing stage when hardening occurs. It is therefore proportional to concrete strength and is expressed as:

$$\varepsilon_{ca}(t) = \beta_{as}(t) \varepsilon_{ca}(\infty), \tag{4}$$

where $\varepsilon_{ca}(\infty)$ is a linear function of concrete strength and $\beta_{as}(t)$ is an exponential function of time accounting for the reduced variation over time of $\varepsilon_{ca}(t)$.

The drying shrinkage $\varepsilon_{cd}(t)$ develops much more slowly, because drying needs time. Its variation over time is expressed as:

$$\varepsilon_{cd}(t) = \beta_{ds}(t, t_s) k_h \varepsilon_{cd,0}, \tag{5}$$

where $\beta_{ds}(t, t_s)$ is a function of time taking account of the long time needed by drying since its start at time t_s , $\varepsilon_{cd,0}$ is a coefficient taking account of relative humidity RH and notional size h of the cross section, that is the ratio h of the double of the cross-sectional area A_c over the perimeter u in contact with the atmosphere, and k_h is a coefficient depending on the notional size h .

2.1.3 Creep

For service stresses $\sigma_c \leq 0.4 f_{cm}(t_0)$, creep is assumed to be linearly related to stress. The creep strain at time t is as follows:

$$\varepsilon_{cc}(t, t_0) = \frac{\sigma_c(t_0)}{E_{ci}} \varphi(t, t_0), \tag{6}$$

where $\varphi(t, t_0)$ is the creep coefficient and E_{ci} is the elastic modulus at the age of 28 days.

Therefore, by adding the deformation $\sigma_c(t_0) / E_{ci}(t_0)$ at the time of loading t_0 to the creep strain, one obtains the stress-dependent strain:

$$\varepsilon_{cc}(t, t_0) = \sigma_c(t_0) \left[\frac{1}{E_{ci}(t_0)} + \frac{\varphi(t, t_0)}{E_{ci}(t_0)} \right] = \sigma_c(t_0) J(t, t_0), \tag{7}$$

where $J(t, t_0)$ is the creep compliance.

Equations (6) and (7) depend on the creep coefficient $\varphi(t, t_0)$ whose expression is as follows:

$$\varphi(t, t_0) = \varphi_0 \beta_c(t - t_0), \tag{8}$$

where φ_0 is defined as the notional creep coefficient and $\beta_c(t - t_0)$ describes the evolution of creep as a function of the concrete age t (expressed in days) referred to the concrete age t_0 at loading (also expressed in days). Notional creep is defined as:

$$\varphi_0 = \varphi_{RH} \beta(f_{cm}) \beta(t_0), \tag{9}$$

where φ_{RH} depends on relative humidity RH , notional size h of the cross section, and concrete strength, $\beta(f_{cm})$ is an hyperbolic function of $\sqrt{f_{cm}}$, and $\beta(t_0)$ is an hyperbolic function of $(1 + \sqrt{t_0})$.

2.1.4 RILEM Model B3

Similar to the previous sections, the creep model defined by the RILEM Model B3, as well as the variation with time of the elastic modulus and shrinkage, is described in the following subsections (Bazant and Baweja 1996).

2.1.5 Elastic Modulus

Considering $E(28)$ as the concrete elastic modulus at 28 days, the expression of the elastic modulus as a function of time is as follows:

$$E(t) = E(28) \left(\frac{t}{4 + 0.85t} \right)^{\frac{1}{2}}. \tag{10}$$

2.1.6 Shrinkage

Shrinkage strain as a function of time is expressed as:

$$\varepsilon_{sh}(t, t_0) = -\varepsilon_{sh\infty} k_h S(t), \tag{11}$$

where $\varepsilon_{sh\infty}$ is the long-term value of ε_{sh} for $t \rightarrow \infty$, k_h is a humidity-dependent parameter, and $S(t)$ is a time-dependent function defined as:

(See figure on next page.)

Fig. 3 Pictures of the Navile Bridge: **a** global view, **b** central joint and **c** cantilever in the proximity of the abutment *F*.

$$S(t) = \tanh \sqrt{\frac{t - t_0}{\tau_{sh}}}, \tag{12}$$

where t_0 is the time at which drying starts acting and τ_{sh} is a size parameter that is proportional to the square of the volume-to-surface ratio of the concrete member.

2.1.7 Creep

Creep is modeled in the RILEM Model B3 by first introducing creep compliance, whose general definition is given in Eq. (7). Creep compliance is defined by RILEM Model B3 as:

$$J(t, t') = q_1 + C_0(t, t') + C_d(t, t', t_0), \tag{13}$$

where q_1 is instantaneous deformation, $C_0(t, t')$ is basic creep compliance, and $C_d(t, t', t_0)$ is drying creep.

The total basic creep compliance is defined as:

$$C_0(t, t') = q_2 Q(t, t') + q_3 \ln [1 + (t - t')^n] + q_4 \ln \left(\frac{t}{t'}\right), \tag{14}$$

where:

$$Q(t, t') = Q_f(t') \left[1 + \left(\frac{Q_f(t')}{Z(t, t')}\right)^{r(t')} \right]^{-\frac{1}{r(t')}} \tag{15}$$

with:

$$r(t') = 1.7(t')^{0.12} + 8, \tag{16}$$

$$Z(t, t') = (t')^{-m} \ln [1 + (t - t')^n], \tag{17}$$

$$Q_f(t') = \left[0.086(t')^{\frac{2}{9}} + 1.21(t')^{\frac{4}{9}} \right]^{-1}. \tag{18}$$

The additional creep due to drying is defined as:

$$C_d(t, t', t_0) = q_5 \left[\exp \{-8H(t)\} - \exp \{-8H(t'_0)\} \right]^{\frac{1}{2}}, \tag{19}$$

where if $t > t'_0$ then $t'_0 = \max(t', t_0)$, otherwise $C_d(t, t', t_0) = 0$, where t'_0 is the time at which drying and loading first act simultaneously with:

$$H(t) = 1 - (1 - h)S(t) \tag{20}$$

and $S(t)$ defined as in Eq. (12).

2.2 Relaxation

The relaxation of prestressing tendons was calculated in accordance with the formulation of Eurocode (2004), where the relaxation loss is calculated as:

$$\frac{\Delta\sigma_{pr}}{\sigma_{pi}} = c\rho_{1000} \left(\frac{t}{1000}\right)^{0.75(1-\mu)}, \tag{21}$$

where σ_{pr} is the absolute value of the relaxation losses, σ_{pi} is the absolute value of the initial prestress, t is the time after tensioning expressed in hours, ρ_{1000} is the value of the strand relaxation losses at 1000 h after tensioning at a temperature of 20 °C, and c is a coefficient depending on the ratio $\mu = \sigma_{pi}/f_{ptk}$ and on the strand class. For class 2 (strands with low relaxation, such as those used for the Navile Bridge), its expression is $c = 0.66e^{9.1\mu}$. The value of ρ_{1000} is obtained from experimental tests under laboratory conditions, but if no experimental tests are available, ρ_{1000} can be assumed to be 2.5% for strands in class 2. Equation (21) allows us to calculate the evolution over-time of relaxation along the cable and therefore of each cable element when modeling the prestressed structure by finite elements.

3 Description of the Navile and Sa Pruna Bridges

The Navile and Sa Pruna Bridges are two box girder bridges built in Sardinia between 1990 and 1994. The two bridges are constructed by repetition of the same balanced cantilever and are therefore very similar to one another because they only differ by the number of spans, that is, by the number of balanced cantilevers (Fig. 3a).

The Navile Bridge consists of 8 spans with a total length of 560 m, whereas the Sa Pruna Bridge consists of 10 spans with a total length of 700 m. The static schemes adopted are the same for both bridges, consisting of continuous beams interrupted by a joint (internal hinge) in the middle point (Figs. 3b and 4b), with cantilevers in the proximity of the abutments connected to the shoulder through a floating slab (Fenu et al. 2019), as shown in Fig. 3c and in Figs. 4a, b

The cross-sectional height and width of the superstructure are 4.5 m and 7 m, respectively, with a superior slab width of 13 m. The thickness of the superior slab varies between 0.24 m and 0.41 m, and the thickness of the inferior slab varies between 0.70 and 0.20 m, depending on the position of the segment. All the segments have relatively slender webs with a thickness of 0.30 m. The diameters of the horizontal



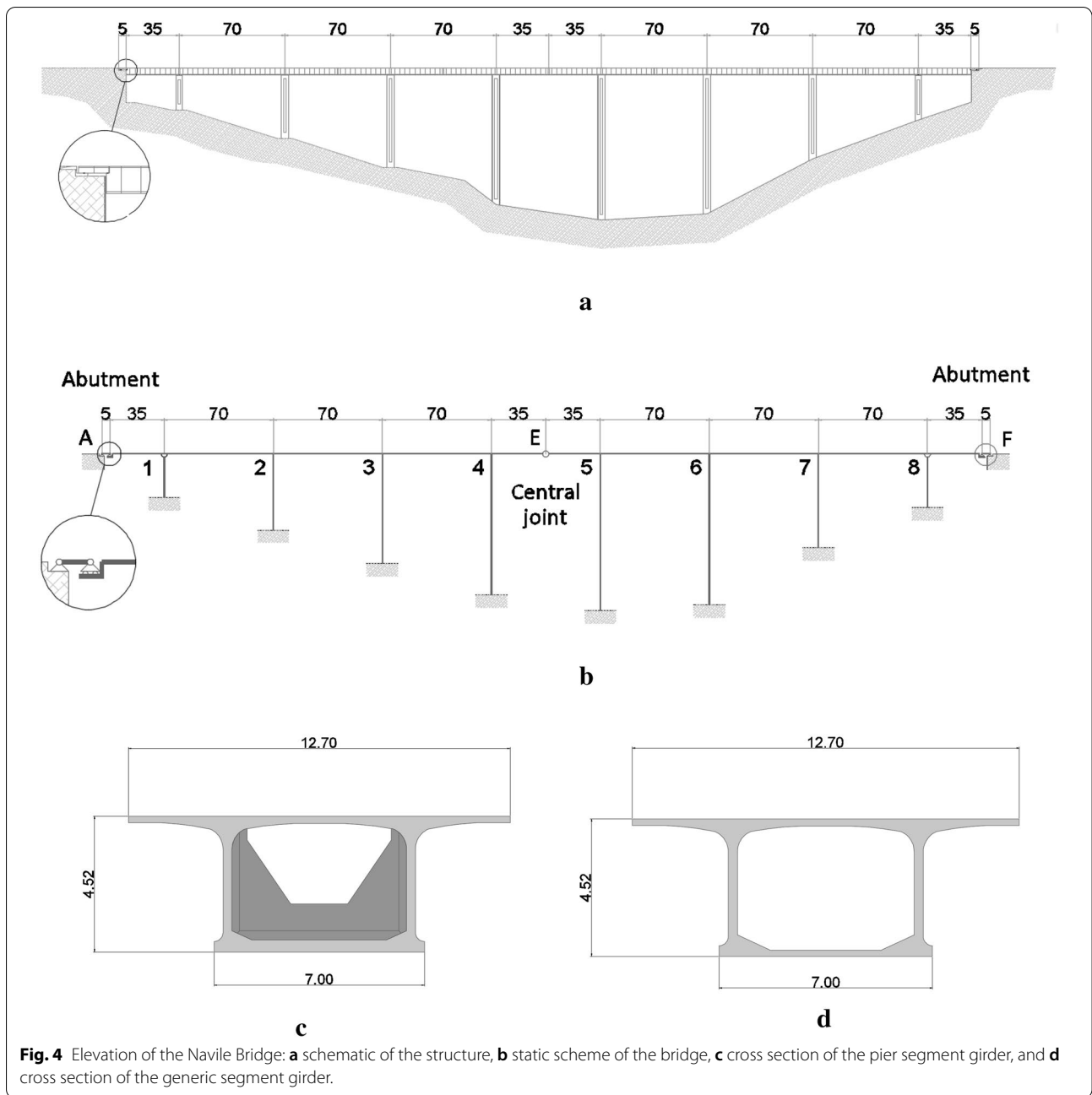
a



b



c



longitudinal reinforcements in the upper and lower slabs vary between 12 and 10 mm with 250 mm spacing; the diameter of the horizontal longitudinal reinforcements of the web is 12 mm with 250 mm spacing. The vertical reinforcement of the web consists of two vertical bars with 14 mm diameter and 165 mm spacing. Pretensioning tendons with 15 strands with 200 mm² of cross-sectional area were used. The pier segment was joined to the pier through temporary pretensioned cables. In the construction stages, top internal

cantilever tendons are provided in the upper flange, while continuity tendons are provided in the bottom flange, which are posttensioned once the center segment of the span is cast.

4 Description of the Typical Launch of Balanced Cantilever Bridges

The structural scheme of segmental bridges obtained by repetition of the same balanced cantilevers (modular cantilever bridge) simplifies their launch for symmetry

reasons, as in the bridge types under consideration in this study. This is the main justification in designing this type of bridge, whose moments, notwithstanding the bridge symmetry and the use of the same cantilever, are not effectively balanced, thus negatively affecting their long-term behavior.

These prestressed continuous box girder bridges are launched through the precast segmental construction technique (overhead method) (Dongzhou and Bo 2019). The precast span-by-span bridge construction method allows a very high speed of construction, which is true if the same balanced cantilevers are used. The launching approach described herein is often utilized in conjunction with an erection truss (overhead erection gantry) for placing the precast segment into position. This construction approach is particularly suitable in the case of long viaducts with spans of similar length.

During the construction stages, the structure is subjected to considerable stress and to strong variations in strain caused by the launching gantry shift, as the weight of the launching gantry is comparable with the permanent loads of the bridge. To compensate for the long-term deflections, upward displacements during cantilevering are imposed to reach a final straight configuration of the bridge. The cantilever launching gantry can move along the viaduct, allowing implementation of the segments.

Considering the specific case of the modular precast cantilever Navile Bridge, a launching gantry weighting 178 tons has been employed; each cantilever arm consists of 11 segments, each 3.35 m long. The segments are arranged at intervals of 3 days. Figure 5 shows some of the construction sequence phases; segments were installed utilizing a temporary prestress necessary to introduce the final prestress on the structure. Figure 5a shows the placement of the pier segment for the first pier; temporary pretensioned cables were used to join the pier segment to the pier to allow the casting of the first span of the bridge, as shown in Fig. 5b. Once the first span has been completed, a temporary pillar is placed in correspondence with the abutment (Fig. 5c) to allow the subsequent shift of the gantry, as shown in Fig. 5d; the position of the gantry allows the placement of the second pier segment, which is permanently joined to the pier and consequently allows the shift of the gantry on the second pillar with the casting of the second span. After the erection of the end span segments of the second span and the tensioning of the bottom continuity tendons, both the temporary pillar in correspondence with the abutment and the temporary pretensioned cables utilized to join the pier segment to the pier are removed to reach the final static configuration of the bridge, thus allowing the shift of the gantry, as shown in Fig. 5f. After this

phase, the subsequent construction stages can continue similarly until the construction end. For the sake of brevity, the subsequent launching phases are not described in the following, since the subsequent steps until the completion of the bridge are similar to the stages previously described. Figure 5g, illustrates the balanced cantilever scheme utilized for the launch of the bridge. During bridge construction, the symmetric cantilever arms have been modularly repeated in space aiming to simplify the launching procedure. Nevertheless, this modular structural scheme is unbalanced in correspondence with the bridge abutments and the central mid-span joint, thus leading to a disequilibrium in the final structural configuration.

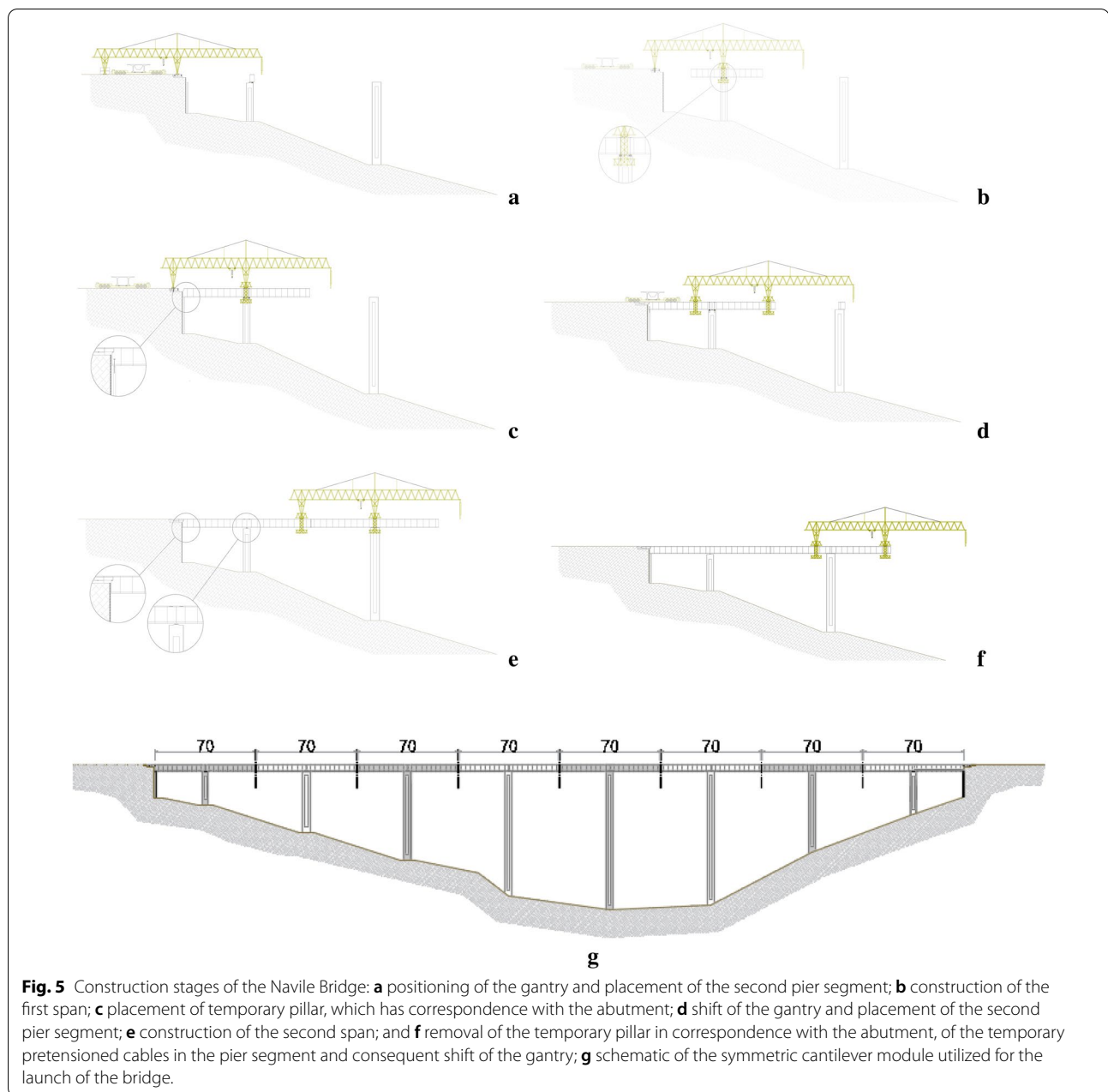
5 Retrofitting of Unbalanced Cantilever Bridges

If not suitably balanced, segmental cantilever bridges can exhibit high creep deflections, which sometimes can evolve indefinitely. Besides causing severe inconveniences and discomfort to traffic, these high deflections can even lead the bridge to collapse, as it happened in the case of Palau bridge (Bazant et al. 2008). For all these reasons, retrofit interventions are often necessary, as reported in several cases in the scientific literature (Neulichedl et al. 2008; Svoboda et al. 2019).

The two cantilevers of Palau bridge were originally connected with a sliding hinge, but this connection type has proved to be unsuitable to prevent creep deflections even in other cantilever bridges. Therefore, in the retrofitting phase, it was decided to change the structural scheme of the bridge by eliminating the mid-span hinge. The bridge static scheme was transformed into a continuous beam by means of external prestressing applied at the girder bottom in the span region across the mid-span hinge, as well as at the top. Unfortunately, the retrofit intervention (completed in July 1996) probably accelerated the collapse (26 September 1996), as investigated by some authors (Bazant et al. 2008; Burgoyne and Scantlebury 2008).

Another cantilever segmental bridge suffering excessive creep deflections was the one over Rio Sinigo (Granata and Arici 2013), with very low span over deflection ratio, only slightly higher than that of Palau bridge (cfr. Section 1). Since after 20 years the huge creep deflections tended to increase indefinitely, in 2005 it was decided to retrofit it (completed in 2008) (Neulichedl et al. 2008). The unfavorable span over deflection ratio similar to that of Palau bridge suggested not to try to retrofit the bridge through external prestressing, but to support the bridge by means of an under deck cable system.

Resia bridge over the Isarco river in Bolzano, Italy, is a concrete bridge of the late'40 with a "Gerber" scheme



on three spans of, respectively, 37.15, 37.70, and 37.15 m; a box girder cross section is used for the simply supported central span whether the end spans are composed by parallel beams supporting a concrete slab (Siviero et al. 2006). The crack pattern showed a defectiveness state affecting many parts of the structure mainly due to shear at the bearings and due to bending moments at central mid-span, confirmed by static and dynamic tests and numerical analyses. The bridge was therefore retrofitted through the following phases: (a) replacing the existing bearings; (b) installing new prestressing cables

to counteract the effects of shear and bending; and (c) using CFRP (Carbon Fiber-Reinforced Polymer) for shear forces and in the anchorage zones to absorb high-stress concentrations.

The first use of external prestressing dates to 1936 and is due to Dischinger, who realized a prestressed concrete bridge in Aue, Germany (Menn 2012). Retrofitting through external prestressing was first used in 1967 to refurbish a steel bridge (1889) in Aarwangen, Switzerland (Mueller 1969). This technique is now largely used to retrofit prestressed concrete bridges, including

segmental bridges, where external tendons can be easily placed inside the box girder. Nevertheless, in case of cantilevers with creep deflections indefinitely evolving in time, some authors note that external prestressing is not always effective in counteracting deflection evolution due to creep (Bazant et al. 2008). Also, in the case of modular segmental double cantilever bridges, the use of prestressing to retrofit the bridges as a counter against the indefinite evolution of creep deflections is not always applicable. This is the case of the two similar segmental bridges built in Sardinia in the '90 of the past century, the Sa Pruna and Navile bridges. Both bridges experienced high deflections at central mid-span, as well as at their ends.

In Navile bridge, the deck displacements at the cantilever ends of the lateral and central spans have shown to indefinitely evolve over time. Their evolution would have been in accordance with what could be expected if realistic numerical simulations had been considered. A realistic numerical simulation could have highlighted the unbalanced structural scheme of the bridge (Bazant et al. 2008; Granata and Arici 2013) not suitable to control the increase in time of the peaks of the negative moments over the piers adjacent to both the lateral and the central spans (Giaccu et al. 2012), as well as the long-term deflections at the end span ends and at central mid-span (Bazant et al. 2008), whose magnitude was becoming incompatible with the bridge service conditions (Bazant et al. 2008).

Moreover, the presence of the internal hinge between the girder and the first pillar and the presence of the floating slab for connection between the bridge deck and abutment caused further disequilibrium of the continuum beam, furtherly increasing cantilever deflections and negative moments on the beams over the end piers (Giaccu et al. 2012).

High deflections occurred at the cantilever free ends and at mid-span of the central span after only 2 years. Moreover, as a counter to this drawback, several ordinary maintenance works (filling with asphaltic concrete) have been carried out on the two lateral cantilevers, aiming to restore the elevation gaps occurred due to the remarkable differential displacements. The actual displacements corresponding to abutments *A* and *F* after 2 years were 11 and 20 cm, respectively, while at the mid-span joint, the displacement was 12 cm. As a result of this detrimental intervention, deflections suddenly increased dramatically owing to the added permanent load, and long-term deformations continued to increase. After approximately 10 years, a slight decrease in the displacement trend slope was noted, but the displacements increase due to long-term effects continued without stopping

even after 22 years. New extraordinary maintenance interventions were, therefore, necessary to replace the viability of the bridge by varying the static scheme of the structure, introducing new constraints, new tendons, and carbon fiber reinforcements on the structure (Lavorato et al. 2015, 2017; Xue et al. 2018). In fact, even after two decades, cantilever long-term deflections tended to indefinitely evolve with time. This trend cannot be inverted unless the displacements of the free end of the cantilevers (or of points close to them) are prevented.

Retrofit interventions aimed at containing these drawbacks were therefore necessary. The intervention works are summarized in Fig. 6 and consist of different phases as described below.

Two new auxiliary pillars (height 4.5 m) have been introduced in correspondence with the end of the two cantilevers to stop their end displacements; the auxiliary pillars have been placed adjacent to the existing bridge abutment since its distance from the abutment is only 5 m; moreover, an upward displacement was imposed at the free end of the two cantilevers. The imposed upward displacement was chosen to make the support immediately effective, and the magnitude of the imposed displacement (1 cm) was chosen to not excessively decrease the negative moments along the cantilever and not to create positive moments along the span under a permanent load.

It must be noted that the newly introduced support and the subsequent upward displacement allow a reduction in the negative bending moments along the cantilever and, in particular, the remarkable peak negative moments over the pier (refer to the next section, e.g., Figs. 10 and 11).

The presence of the abovementioned interventions involves, under service conditions, positive bending moments in the cantilever (due to the presence of live loads), which in turn are not properly designed for bearing positive moments. It is therefore important that retrofit interventions include a reinforcement system at the intrados of the cantilever. Since, from a practical standpoint, it is evident that adding steel rebars was difficult to implement, the application of a composite reinforcement at the intrados surface was chosen.

In the last decade, fiber-reinforced polymers (FRPs) have been largely used to meet this aim, even if, now, the use of cement composites and fiber-reinforced mortars appears to be increasingly used (Aymerich et al. 2020; Fenu et al. 2015; 2016; Kruszka 2015). In the case of the Navile Bridge, carbon FRP was used, with carbon fibers with $E=270$ GPa and $f_k=2700$ MPa. The total resistant area of carbon fiber was 1932 mm^2 . It was applied in strips with a total width of 7000 mm, thickness of

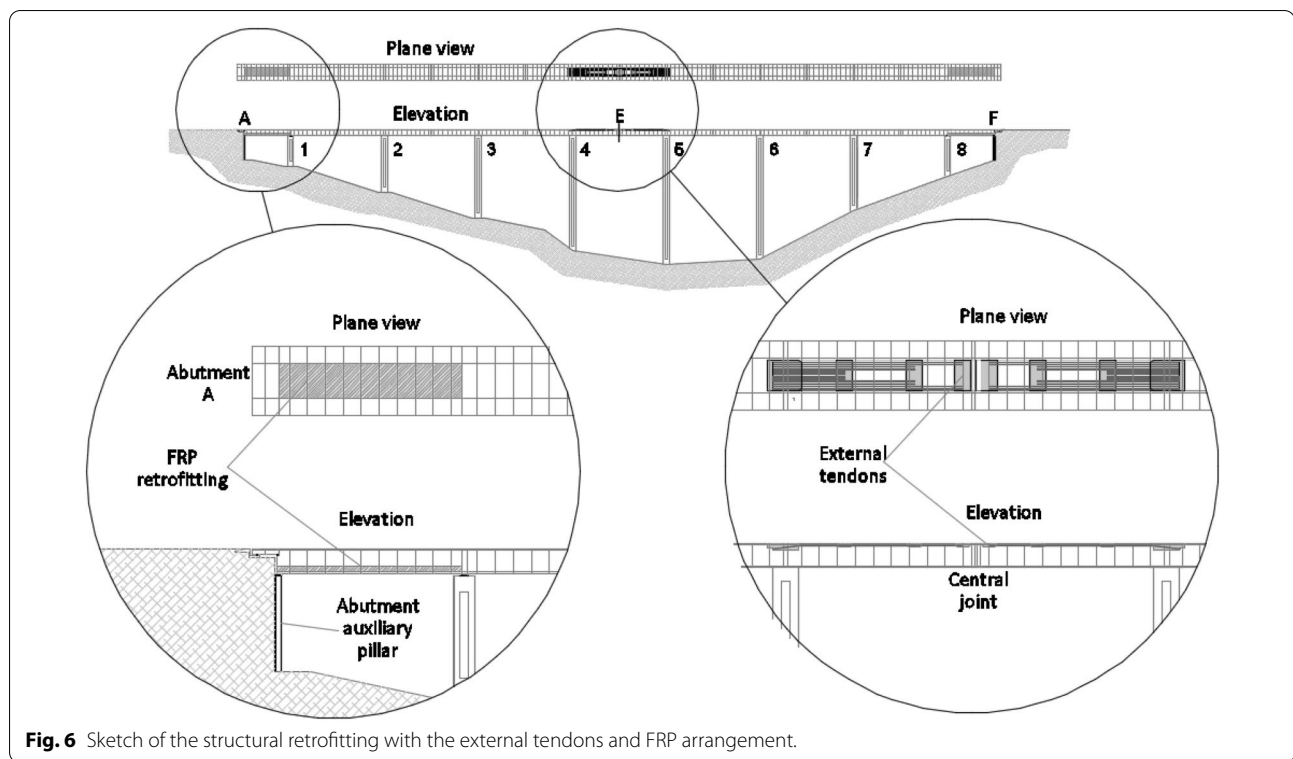


Fig. 6 Sketch of the structural retrofitting with the external tendons and FRP arrangement.

0.28 mm, and bond length of 100 mm. After applying the FRP reinforcement, the moment of resistance of the beam sections against the positive moments was 56,900 kNm, which is only slightly higher than the maximum estimated positive moment under service loads.

Furthermore, retrofit interventions were necessary on the central span of the bridge due to the remarkable displacements that occurred at the central mid-span joint. This structural discontinuity resulted in substantial deflections corresponding to the hinge. Similar to what happened in the proximity of the abutments, joint deflections exhibited an unusual trend, with creep deformations continuously increasing overtime, even after more than twenty years from the construction date.

Vertical deflections have been counteracted by introducing new unbounded prestressing tendons in the intrados of the girder upper slab (refer to Fig. 7). In the present case, straight tendons were symmetrically positioned in the upper part of the cantilever with a constant center distance and with an equal distance from the intrados. A total of twelve tendons were utilized, each one with 9 strands 06" with cross-sectional area $A_p = 150 \text{ mm}^2$ and tensile strength $f_{pu} = 1860 \text{ MPa}$. The initial tension force in the cables was 1800 kN, that is, the initial tensile stress in the strands was 50% of the tensile strength. All the cables were symmetrically placed side by side just

below the girder flange and with the same depth from the extrados.

The post-tensioning forces in the cables were applied by a tendon anchorage positioned in the pier head segment diaphragm (Fig. 8). After 11 m from the pier centerline, the four central cables were the first ones to be anchored to their anchor blisters positioned in a transverse rib where the remaining 8 cables were instead deviated to conform to the very slow horizontal curvature of the beam. After 13 m from that rib, the other four cables were anchored to another transverse rib, while the last four cables were still slightly deviated to be anchored to a third transverse rib close to mid-span (central joint). Symmetrically, the same retrofit measure was employed in the other balanced cantilever of the central span. A further effect of this retrofit measure is that the application of prestressing forces leads to a reduction in the substantial negative moments over the piers of the central span, as shown in Fig. 10.

6 Finite Element Analysis

Finite element analysis was performed with the finite element software Midas Civil (MIDAS 1989). According to the classical theory of bending, a linear Timoshenko beam element model was used. The limits of this model are well known in the literature (Bazant et al. 2008), Nevertheless, a FE beam model was used and aimed to

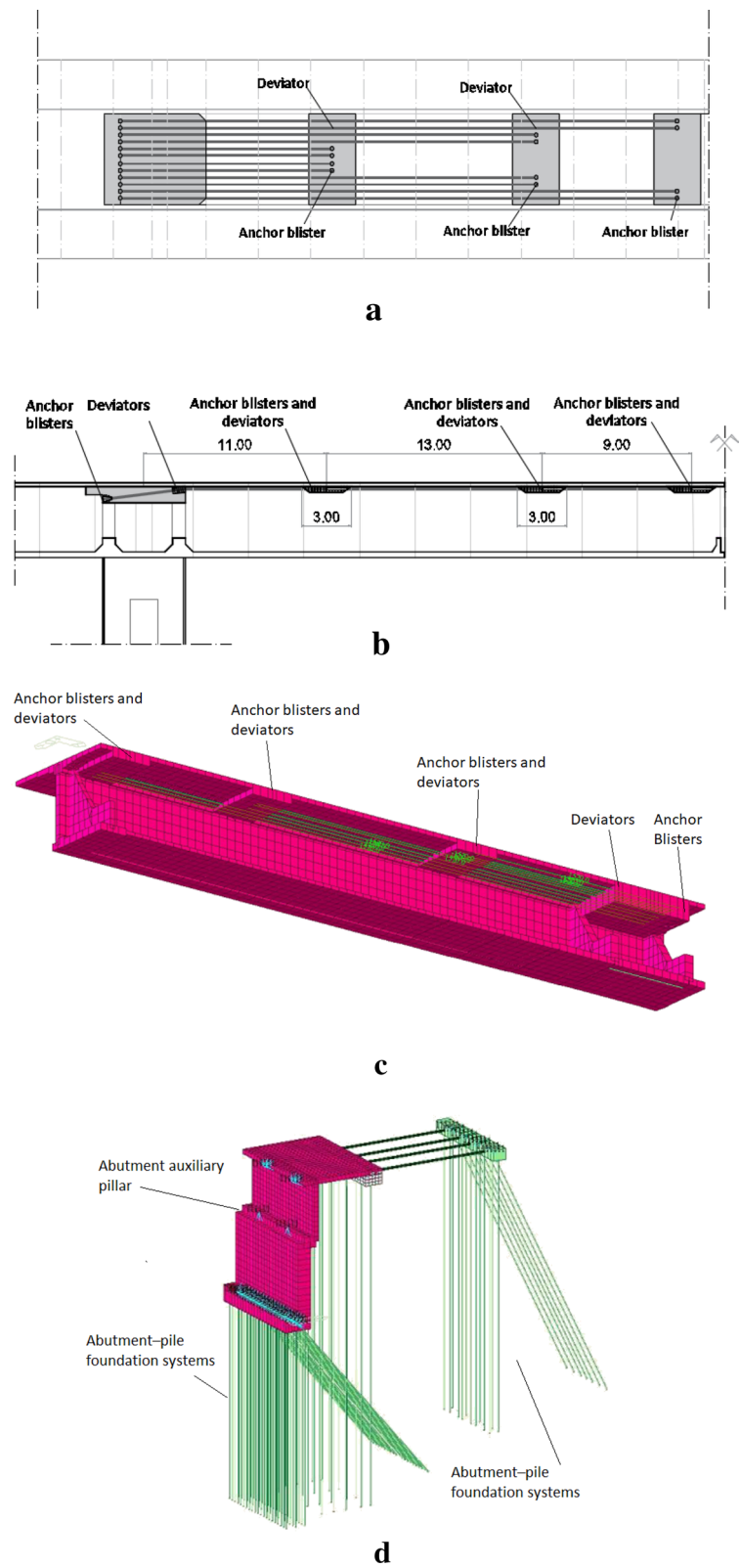


Fig. 7 Sketch of maintenance interventions and structural retrofitting of the external tendons in proximity of the central joint, **a** plane view, **b** elevation, **c** 3D view and **d** 3D view of the abutment auxiliary pillar.

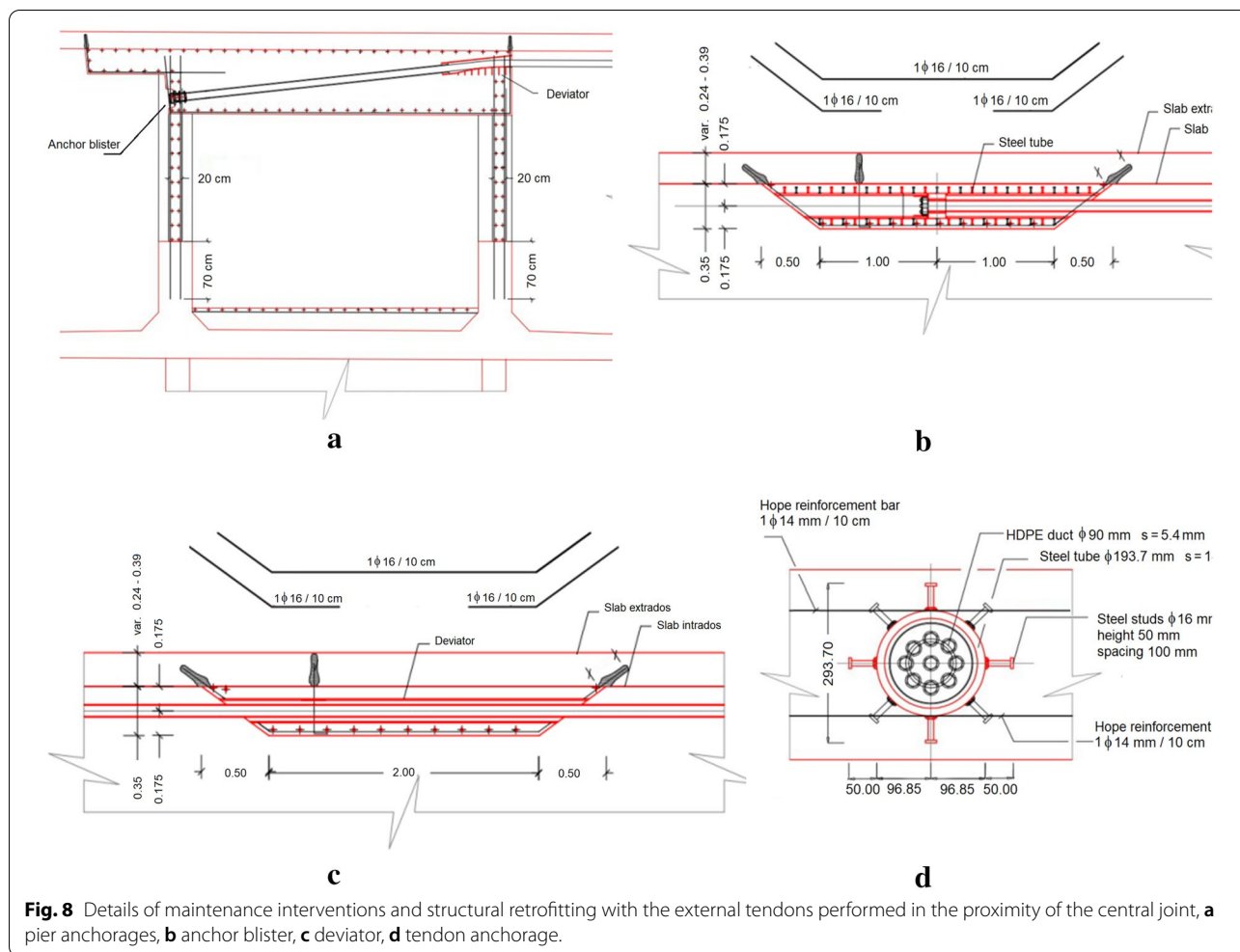


Fig. 8 Details of maintenance interventions and structural retrofitting with the external tendons performed in the proximity of the central joint, **a** pier anchorages, **b** anchor blister, **c** deviator, **d** tendon anchorage.

simulate the launching phases and long-term behavior of the bridge. The choice of the beam element model is motivated by the complexity of the structure, which includes a total of 168 segments and 206 construction stages, with 1324 different tendon profiles. The model would have been furthermore complex if creep nonlinearity was not neglected. Fortunately, in the majority of engineering applications, including the case under consideration, for service limit states (SLS), linear creep models can be considered, provided that compressive stresses in concrete are lower than 40% of concrete compressive strength. Of course, beam elements neglect some features of beam behavior when creep occurs (Bazant et al. 2008). For instance, due to creep, plane sections do not remain planar, but this feature cannot be taken into account by FE models implemented with beam elements. Moreover, using beam models, prestressing is applied through equivalent loads that neglect the large stress and strain concentrations caused in each section by the interaction between the cables and concrete. Nevertheless,

as previously mentioned, for most of practical engineering applications, linear creep models coupled with beam modeling can be properly utilized for bridge design, provided that the above limitations are taken into account (Bazant et al. 2008).

Numerical analysis was performed beginning with the initial step of the bridge launching, taking into account, step by step, each increase in load introduced by new segments, by new tendons, and by the shift of the launching gantry. The launch of this type of bridge involves the consideration of many concrete characteristics, with reference to all the concrete properties evolving overtime owing to the high time dependence of the static behavior of the entire structure. The evolution of material parameters, such as elastic modulus, shrinkage, creep, and relaxation, are described in the next section, according to the design codes CEB-FIP Model Code 2010 (2012), RILEM model B3 -(Bazant and Baweja 1996), and Eurocode 2 (2004). Since all the launching stages are affected by the time-dependent characteristics of the material

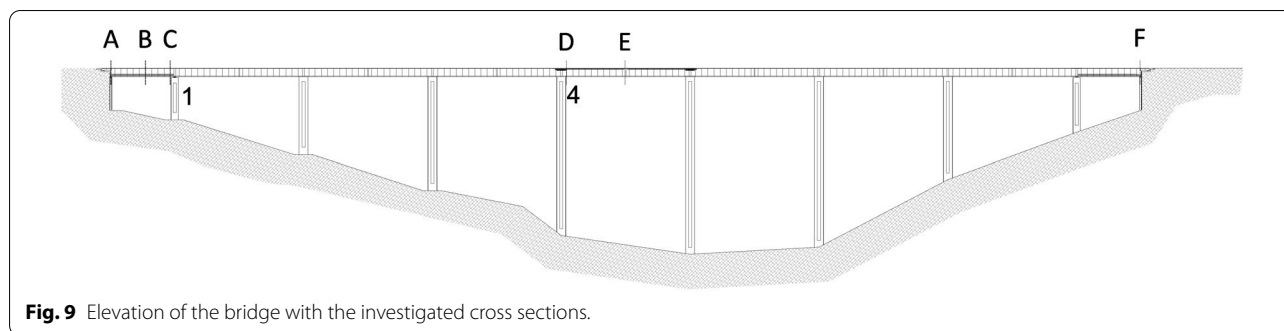


Fig. 9 Elevation of the bridge with the investigated cross sections.

parameters, the simulation by the FE model must respect the actual time of each launching phase. For each construction phase, time is computed considering that the segments are arranged by the launching gantry at intervals of 3 days. To compensate for the long-term deflections, the upward displacements during cantilevering are imposed to reach a final straight configuration of the bridge.

It is worth noting that when modeling a structure whose time-dependent behavior highly affects its performances, an accurate estimation of creep and shrinkage properties to be used in the FE has to be done to improve the accuracy of the structural model (Bazant and Baweja 2000). For this reason, in this study the creep effects have been accurately determined using two of the more representative linear creep models available in the scientific literature and implemented in beam FE models. The beam model is less accurate than detailed 3D FE model with solid elements, but it is much simpler to be implemented and needs much less computation costs. The reliability of this simple beam FE model in the case of modular segmental balanced cantilever bridges is herein investigated.

7 Results

A FE model has been implemented to analyze the time-dependent behavior of precast segmental bridges, and the results are discussed herein.

The FE model has analyzed the actual time-dependent behavior of the bridge at all the construction phases, including the retrofit interventions as well as under the service conditions, both before and after retrofitting. In particular, in Navile bridge the time-dependent response of the bridge has shown to be more critical in some specific sections. In Fig. 9 it is shown the elevation of the bridge with the investigated cross sections.

The bridge time-dependent behavior has been analyzed at different times after the construction end using the creep models of both the CEB-FIP MC 2010 and of the RILEM Model B3.

In Fig. 10, the evolution of the bending moments calculated accounting for these two creep models at different times has been compared. Figure 10a, b compares the bending moments before the retrofitting interventions at the beginning of the serviceability life of the bridge, and after 22 years from the construction end. Similar comparison is, respectively, made in Fig. 10c, d just after the retrofit intervention and 30 years later.

The relevant peaks of the bending moments in correspondence with the pillars are more pronounced for the unbalanced cantilevers of the extremity spans and for the central span, that is, in Sects. 1 and 4 shown in Fig. 9, as well as in the symmetrical ones. The evolution in time of the bending moment in Sects. 1 and 4 is shown, respectively, in Figs. 11 and 13.

Figures 10 and 11 show that in section C in correspondence with the pier #1 the relevant increase in the first 22 years of the bridge serviceability life of the negative moment calculated with both creep models is very similar. After the retrofit intervention consisting in erecting an additional pier supporting the cantilever free end at the abutment and after imposing it an upward displacement of 1 cm, the two creep models are shown to give a different response in time: in fact, while the creep effect on the moment obtained through the CEB-FIP MC 2010 in the successive 30 years results negligible, using the RILEM Model B3 the creep effect results in a significant reduction of the negative moment in Sect. 1. The evolution over time of the negative moments obtained through the RILEM Model B3 appears to be more in accordance with the reality than the moment stabilization obtained using the CEB-FIP MC 2010. It is in fact reasonable that after this retrofit intervention, the negative moments continue to decrease over time, that is, due to creep, continue to be affected by the effect over time of the additional support and of the related imposed uplift at the cantilever free end.

Figure 11 shows that the imposed uplift suddenly lowered the substantial negative moments over lateral pier #1 from $-98,000$ to $-83,000$ kNm.

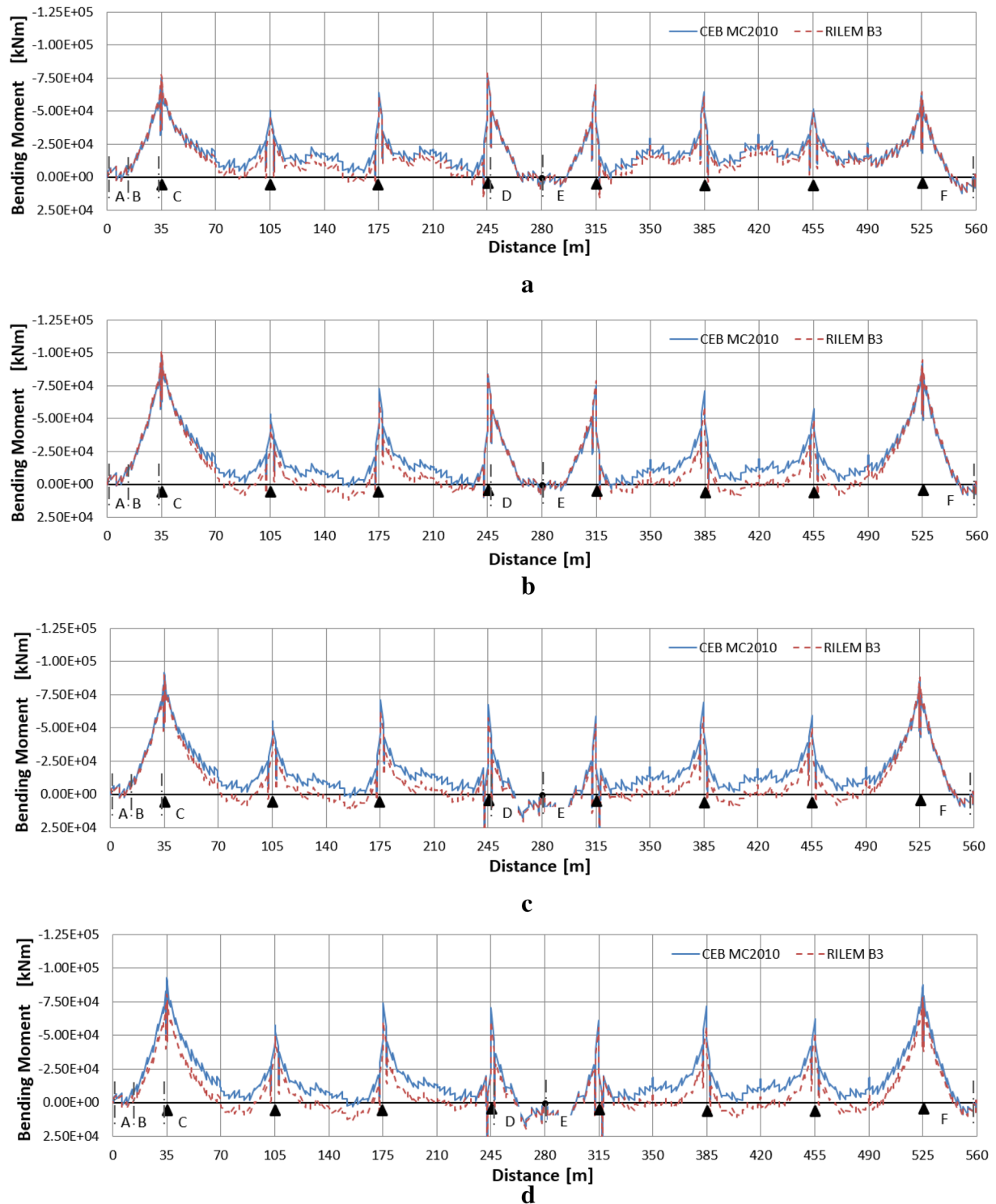
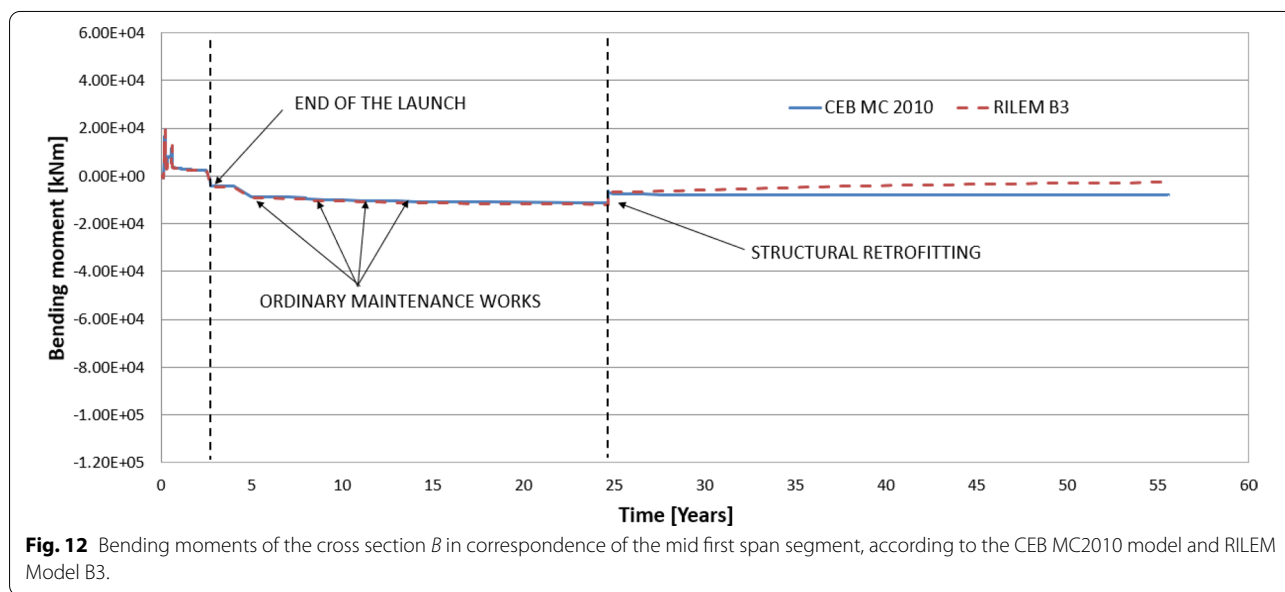
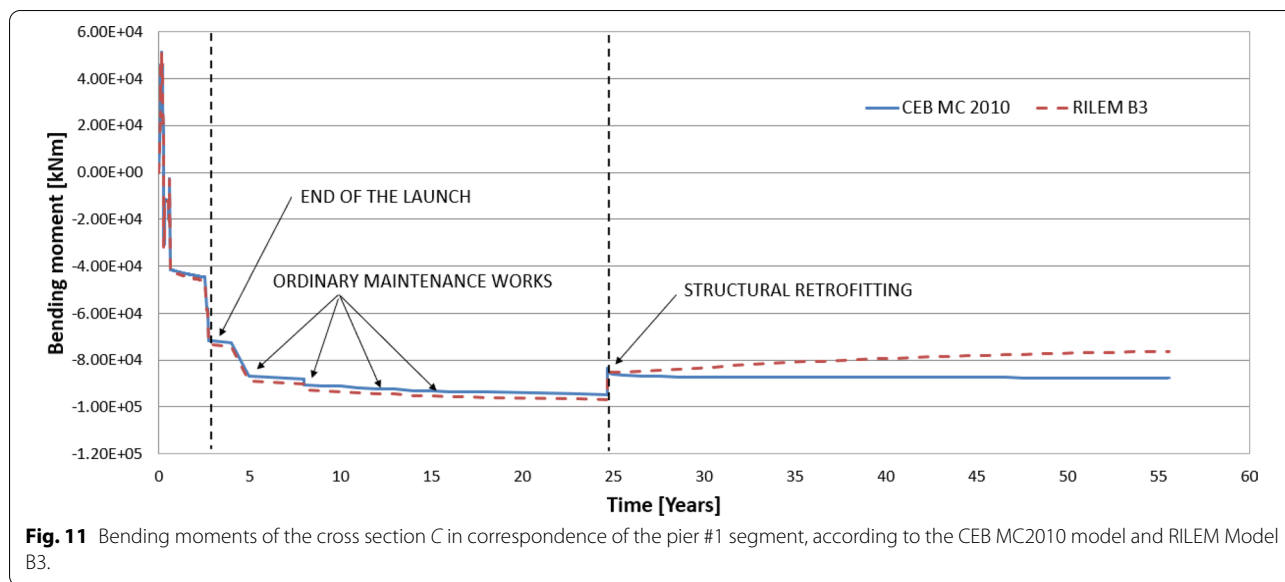


Fig. 10 Bending moment acting on the Navile Bridge deck at different times according the CEB MC2010 model and RILEM Model B3: **a** at the beginning of the serviceability life of the bridge, **b** before the retrofitting interventions, **c** after the retrofitting interventions and **d** 30 years after the retrofitting interventions.

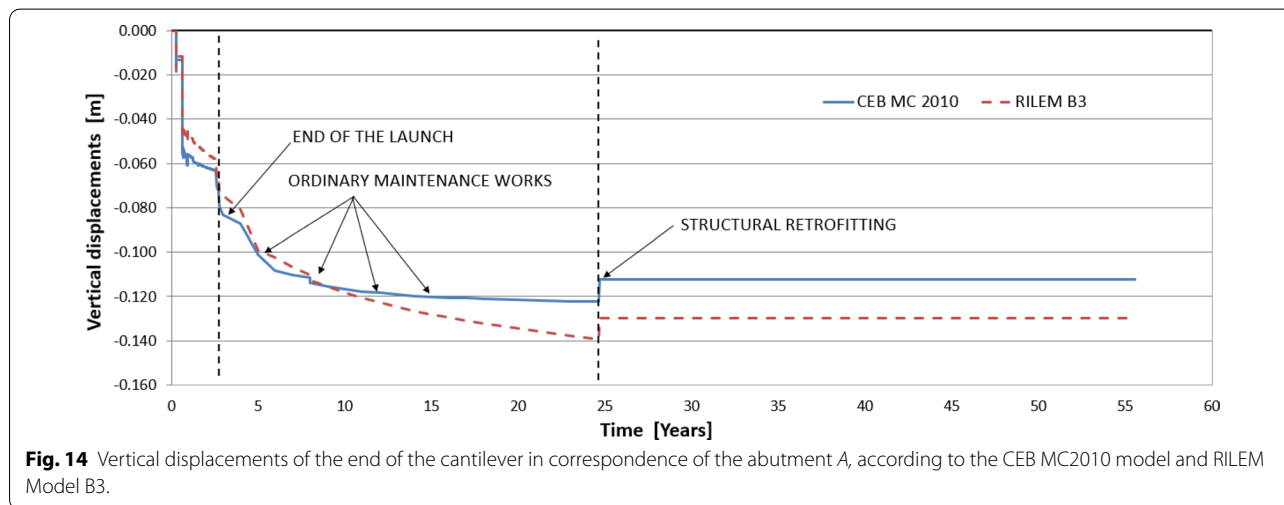
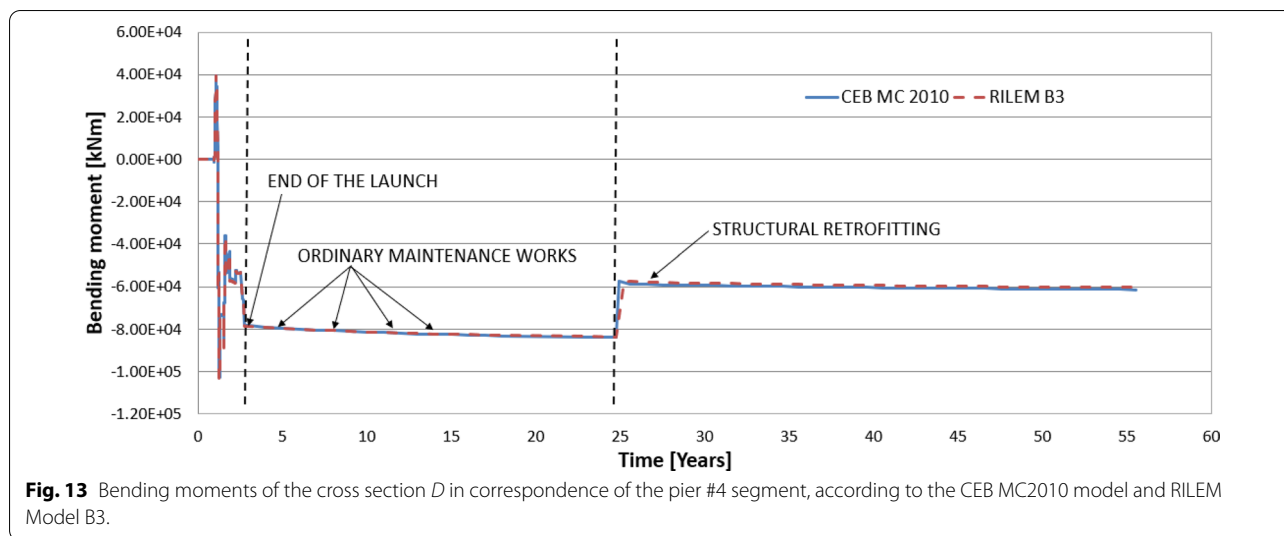


Figures 10 and 12 show that also at mid-first-span cross section B both creep models lead to similar evolution of the bending moment before retrofitting the bridge at the abutments. After the retrofit intervention, there are no significant creep effects evaluated through the CEB-FIP MC 2010, while the use of the RILEM Model B3 leads to a change of the moment in the 30 years after the bridge retrofitting.

This long-term response in the end span is further highlighted at the mid-first-span cross section (see Fig. 12), where the negative moment was almost halved (from - 12,000 to - 7000 kNm), and only RILEM

Model B3 was able to capture the important further reduction over time of the negative moment to - 2500 kNm 25 years after the retrofit intervention.

Figures 10 and 13 show that the different long-term response related to the use of the two creep models is less evident when analyzing the negative moments of the cross section D over the pier #4. In this case, after reducing the negative moment over the pier from - 83,000 to - 59,000 kNm through externally prestressing the upper part of the girder sections to reduce mid-span deflections, both creep models led to a very slight reduction



over time in the negative moment after the retrofit intervention.

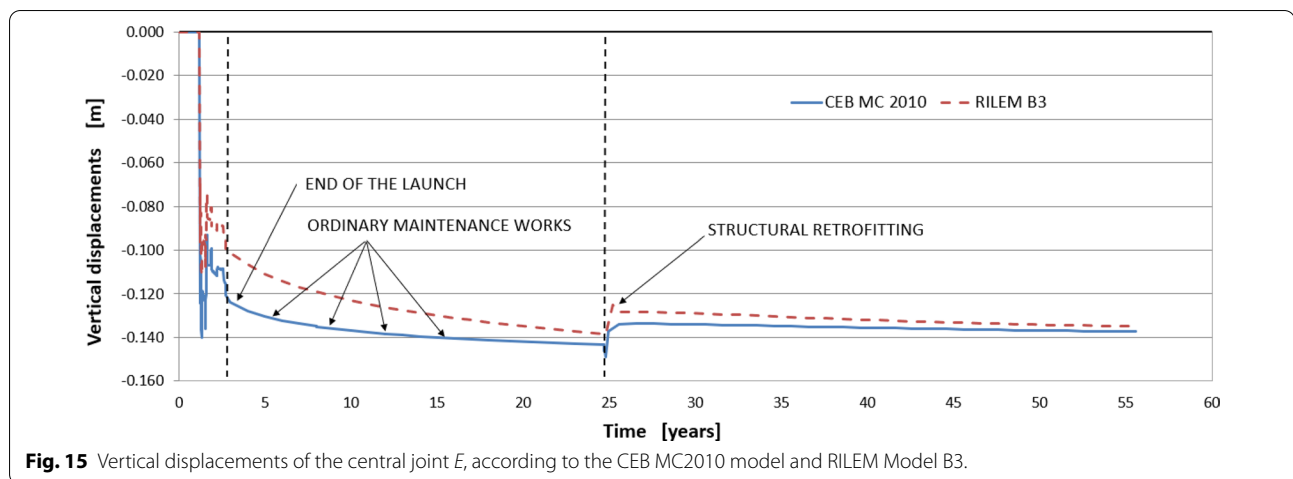
For all considered different times, bending moment diagrams reveal a disequilibrium of the cantilevers that is intrinsic in the static scheme of the bridge, and which in turn cause unexpectedly high long-term vertical deflections incompatible with the service conditions.

Time history of displacements of the cross sections *A* and *E* have been investigated, aiming to evaluate any difference between the considered models and any correspondence with actual displacements. The results are shown in Figs. 14 and 15.

High deflections occurred at the cantilever free ends and at central mid-span after only 2 years (730 days in Figs. 14 and 15). The results obtained by the numerical

model show that without retrofit interventions the displacement increase due to long-term effects would have continued even after 22 years, as can be evaluated also by Figs. 14 and 15 through extrapolating the deflection vs. time plots obtained using the RILEM B3 Model.

The magnitude of these remarkable deflections occurred in correspondence with bridge abutments *A* and *F* (28 and 32 cm, respectively) was not captured by the FE model with the beam elements implemented in this study (13 cm for cantilever ends *A* and *B* and 14 cm for central hinge *E*), but their trend was well predicted by the RILEM B3 creep model, which was able to capture the creep deflection tendency to continue to increase over time (see Figs. 14 and 15). On the contrary, especially at the cantilever end close to the abutment *A* (Fig. 14), the FE model using the CEB-FIP MC 2010 was



not able to capture the indefinite evolution of the cantilever end deflections, that tend to a horizontal asymptote without indefinitely evolving with time. The magnitude of the deflection at central joint *E* after 22 years from the construction end (12.5 cm) was instead captured by both creep models (see Fig. 15).

It is worth noting that the short- and medium-term deflections calculated through the CEB-FIP Model Code 2010 are always higher than those calculated through the RILEM Model B3 (see Figs. 14 and 15), while if deflections evolve for quite long durations, the latter can give higher deflections. The RILEM Model B3 is in fact able to capture the continuous evolution overtime due to creep under some conditions (i.e., structural schemes with unbalanced cantilevers), which can lead deflections to increase indefinitely. The same time displacements trend is confirmed by other authors (Granata et al. 2013) which highlight greater long-term displacements for the RILEM Model B3 than for the creep model of the CEB-FIP MC 2010.

8 Conclusions

This paper focuses on the problem of predicting long-term deflections in segmental prestressed bridges with unbalanced cantilevers. In particular, the case of modular segmental cantilever bridges obtained by subsequently realizing the same double cantilever is analyzed herein. In these cases, it has been observed that creep deformations can evolve indefinitely, with such high deflections that the service conditions are not respected. To simulate the long-term behavior of these segmental bridges, complex tridimensional models with nonlinear creep models could be implemented; nevertheless, this approach involves high costs both in implementing the model and in computation time. Therefore, this approach is difficult to apply in current engineering practice, where simpler

models are generally used. From a practical standpoint, beam modeling of the bridge with beam elements only and linear creep models is therefore advantageous.

A beam FE model has been therefore implemented in this study using two different linear creep models: the creep model proposed by the CEB-FIP Model Code 2010 and the RILEM B3 creep model. A comparison between the results obtained with these two different creep models has been performed. The proposed modeling takes into account of all the construction phases and of the long-term behavior of the bridge before and after the retrofit interventions.

The following conclusions can be drawn from the numerical analysis:

1. In such unbalanced cantilever bridges, creep deflections of the free end of the lateral cantilevers can evolve indefinitely over time.
2. Changing the structural scheme by adding an auxiliary pier to support the free end of the unbalanced cantilever is an effective way to interrupt such an indefinite deflection increase in the end spans, the only effective solution that does not increase the girder depth and does not reduce the span length.
3. The presence of the new support (auxiliary pier) means that the end span must also be reinforced against the positive moments. FRP or cement composites are generally used for this aim.
4. Additionally, creep deflections at the mid-span hinge of the central span can evolve indefinitely over time.
5. In this case, since there is no possibility of adding an auxiliary pier in the central span, deflections can be controlled by suitably applying supplementary pretension to both central span cantilevers.

6. The trend of the deformations is well captured by linear FE models, especially by the RILEM B3 model; however, deformations can be underestimated due to limitations of the beam elements, especially for long-term deflections.
7. The indefinite evolution of the deflection of the cantilever free ends due to creep cannot be stopped by only prestressing applied at the upper part of the cantilever. This retrofit intervention is instead quite effective in the cantilever ends hinged one to the other, as in the central span of the bridge herein considered. In this case, even if creep deflections will continue to slowly evolve over time, their magnitude after 25 years from the retrofit intervention would be approximately 5 mm only.
8. Upper post-tensioning cables of retrofitting interventions are effective in reducing negative bending moments, but less effective in reducing long-term evolution of vertical displacements of the central joint.
9. With respect to the RILEM model B3, the creep model of the CEB-FIP Model Code 2010 tends to overestimate creep deflections in the short term.
10. For all these reasons, even when simple FE beam models are used, in prestressed segmental bridges, the RILEM model B3 appears to be more suited to simulate the long-term behavior of the bridge, in particular when creep deflections are remarkable and tend to evolve indefinitely with time.

Acknowledgements

The authors gratefully acknowledge the financial support from the National Natural Science Foundation of China (Grant No. 51778148) and by "Regione Autonoma della Sardegna" (L.R. n. 3/2008 Rientro Cervelli). Moreover, they are grateful to Eng. Antonio Vincis for kindly supplying the design data of the maintenance interventions and of the structural retrofitting of the examined bridge.

Author's information

GFG (Assistant Professor at Department of Architecture, Design and Urban Planning); DS (Researcher at Department of Architecture, Design and Urban Planning); BB (Full Professor at College of Civil Engineering); LF (Associate Professor at Department of Civil and Environmental Engineering, and Architecture).

Authors' contributions

GFG conceived the study and drafted the manuscript. DS carried out the numerical simulations. LF participated in the design of the study, helped to draft the manuscript and participated in its design and coordination. BB participated in the design of the study, helped to draft the manuscript and participated in its design and coordination. All authors read and approved the final manuscript.

Funding

This research was supported by the National Natural Science Foundation of China (Grant No. 51778148) and by "Regione Autonoma della Sardegna" (L.R. n. 3/2008 Rientro Cervelli).

Availability of data and materials

The datasets used or analyzed during the current study are available from the corresponding author on reasonable request.

Competing interests

The authors declare that they have no competing interests.

Author details

¹ Department of Architecture, Design and Urban Planning, University of Sassari, Palazzo del Pou Salit, Piazza Duomo 6, 07041 Alghero, Italy. ² College of Civil Engineering, Fuzhou University, No. 2 Xue Yuan Road, Fuzhou 350108, Fujian, China. ³ Department of Civil and Environmental Engineering, and Architecture, University of Cagliari, 09124 Cagliari, Italy.

Received: 7 June 2020 Accepted: 29 October 2020

Published online: 11 February 2021

References

- Aymerich, F., Fenu, L., & Loi, G. (2020). FE analysis of the flexural behavior of cementitious composites using the concrete damage plasticity model. In *Proceedings of Italian Concrete Days 2018. ICD 2018. Lecture Notes in Civil Engineering*. Cham : Springer.
- Bazant, Z. P. (1966). *Phenomenological theories for creep of concrete based on rheological models* (pp. 82–109). Prague: Acta Technica CSAV.
- Bazant, Z. P. (1972). Numerical determination of long-range stress history from strain history in concrete. *Material and Structures*, 5, 135–141.
- Bazant, Z. P. (2015). RILEM Model B4 (2015). Model B4 for creep, drying shrinkage and autogenous shrinkage of normal and high strength concretes with multi-decade applicability. *Materials and Structures*, 48, 753–770.
- Bazant, Z. P., & Baweja, S. (1995). Creep and shrinkage prediction model for analysis and design of concrete structures—model B3. *Matériaux et constructions*, 28(180), 357–365.
- Bazant, Z. P., & Baweja, S. (1996). Creep and shrinkage model for analysis and design of concrete structures—model B3 Draft RILEM Recommendation. *Materials and Structures*, 28, 357–365.
- Bazant, Z. P., & Baweja, S. (2000). Creep and shrinkage prediction model for analysis and design of concrete structures: Model B3—short form. In: A. Al-Manaseer (Ed.). *Adam Neville Symposium: creep and shrinkage-structural design effects, ACISP-194*, Am. Concrete Institute, Farmington Hills, Michigan, pp. 85–100.
- Bazant, Z. P., & Chern, J.-C. (1984). Bayesian Statistical Prediction of Concrete Creep and Shrinkage. *American Concrete Institute Journal*, 81, 319–330.
- Bazant, Z. P., & Hubler, M. H. (2014). Theory of cyclic creep of concrete based on Paris law for fatigue growth of subcritical microcracks. *Journal of the Mechanics and Physics of Solids*, 63(1), 187–200.
- Bazant, Z.P., Li, G.H., Yu, Q., Klein, G., & Kristek, V. (2008). Explanation of Excessive long-time deflections of collapsed record-span box girder bridge in Palau. In *8th International Conference on Creep and Shrinkage of Concrete (CONCREEP-8)*, Ise-Shima, Japan.
- Bazant, Z. P., Osman, E., & Thongutha, W. (1976). Practical formulation of shrinkage and creep of concrete. *Matériaux et Construction*, 9(54), 395–406.
- Bazant, Z. P., Sener, S., & Kim, J. K. (1987). Effect of cracking on drying permeability and diffusivity of concrete. *ACI Materials Journal*, 84, 351–357.
- Bazant, Z. P., & Xi, Y. (1994). Drying creep of concrete: Constitutive model and new experiments separating its mechanisms. *Materials and Structures*, 27, 3–14.
- Bazant, Z. P., & Zebich, S. (1983). Statistical linear regression analysis of prediction models for creep and shrinkage. *Cement and Concrete Research*, 13, 869–876.
- Burgoyne, C., & Scantlebury, R. (2008). Lessons learned from the bridge collapse in Palau. In *Proceedings of ICE Civil Engineering 161 November 2008*, 700038, pp. 28–34.
- Carol, I., & Bazant, Z. P. (1993). Viscoelasticity with aging caused by solidification of non aging constituent. *ASCE J. of Engg. Mech.*, 119(11), 2252–2269.
- CEB. (1964). *Recommendations for an international code of practice for reinforced concrete*. Paris: Comité Européen du Béton.
- Chiorino, M. A. (2005). A rational approach to the analysis of creep structural effects. Gardner & Weiss eds. *ACI SP-227*. pp. 107–141.

- Chiorino, M. A., Bazant, Z. P., Fauchart, J., & Jungwirth, D. (1972). Manual structural effects of time—dependent behaviour of concrete, 2-nd Draft, CEB Bulletin d'Information N° 80, 118 pp.
- Chiorino, M. A., & Lacidogna, G. (1993). Revision of the design aids of CEB. Design manual on structural effects of time-dependent behaviour of concrete in accordance with CEB-FIP Model Code 1990. CEB Bulletin d'Information N.215
- Chiorino, M. A., Napoli, P., Mola, F., & Koprna, M. (1984). CEB design manual on structural effects of time dependent behaviour of concrete. CEB Bulletin d'Information n., 142/142bis.
- Dischinger, F. (1939). Elastische und plastische Verformungen bei Eisenbeton-tragwerke. *Der Bauingenieur*, 20, 53–63, 286–294, 426–237, 563–272.
- Dongzhou, H., & Bo, H. (2019). *Concrete segmental bridges, theory, design, and construction to AASHTO LRFD specifications*. Boca Raton: CRC Press.
- EC2. (2004). *Eurocode 2: design of concrete structures Part 1–1: general rules and rules for buildings* (p. 2004). Brussels: EN 1992-1-1, CEN.
- Fanourakis, G. C. (2017). Validation of the FIB 2010 and RILEM B4 models for predicting creep in concrete. *Architecture Civil Engineering Environment*, 95, 95–101.
- Fenu, L., Colasanti, V., Congiu, E., Giaccu, G. F., Lavorato, D., Trentadue, F., & Briseghella, B. (2019). A heuristic approach to identify the steel grid direction of R/C slabs using the yield-line method for analysis. *Advances in Civil Engineering*, 2019, 6017146.
- Fenu L., Forni D., & Cadoni, E. (2015). Energy absorption at high strain rate of glass fiber reinforced mortars. In *11th International Conference on the Mechanical and Physical Behaviour of Materials Under Dynamic Loading, DYMAT 2015, EPJ Web of Conferences, Lugano, Switzerland*.
- Fenu, L., Forni, D., & Cadoni, E. (2016). Dynamic behaviour of cement mortars reinforced with glass and basalt fibres. *Composites Part B*, 92, 142–150.
- Giaccu, G. F., Solinas, D., & Gamberini, G. P. (2012). Time dependent analysis of segmentally constructed cantilever bridge comparing two different creep models. In *Concrete repair, rehabilitation and retrofitting III—Proceedings of the 3rd international conference on concrete repair, rehabilitation and retrofitting, ICCRRR 2012 Cape Town, South Africa*. pp. 1501–1508.
- Glanville, W. H. (1933). Creep of concrete under load. *The Structural Engineer*, 11(2), 54–73.
- Granata, M. F., & Arici, M. (2013). Serviceability of segmental concrete arch-frame bridges built by cantilevering. *Bridge Structures*, 9, 21–36.
- Granata, M. F., Margiotta, P., & Arici, M. (2013). Simplified procedure for evaluating the effects of creep and shrinkage on prestressed concrete girder bridges and the application of European and North American prediction models. *Journal of Bridge Engineering*, 18(12), 1281–1297.
- Kruszka, L., Močko, W., Fenu, L., & Cadoni, E. (2015). Comparative experimental study of dynamic compressive strength of mortar with glass and basalt fibres. In *11th International Conference on the Mechanical and Physical Behaviour of Materials Under Dynamic Loading, DYMAT 2015, EPJ Web of Conferences, Lugano, Switzerland*.
- Lavorato, D., Bergami, A. V., Nuti, C., Briseghella, B., Xue, J., Tarantino, A. M. et al. (2017). Ultra-high-performance fibre-reinforced concrete jacket for the repair and the seismic retrofitting of Italian and Chinese RC bridges. In *COMPADYN 2017—proceedings of the 6th international conference on computational methods in structural dynamics and earthquake engineering*. pp. 2149–2160.
- Lavorato, D., Nuti, C., Santini, S., Briseghella, B., & Xue, J. (2015). A repair and retrofitting intervention to improve plastic dissipation and shear strength of Chinese RC bridges international association for bridge and structural engineering, IABSE symposium report. pp. 1–6.
- Levi, F., & Pizzetti, G. (1951). *Fluage, Plasticite, Precontrainte, Dunod [In French]*, Paris.
- Maekawa, K., Chijiwa, N., & Ishida, T. (2011). Long-term deformational simulation of PC bridges based on the thermo-hygro model of micro-pores in cementitious composites. *Cement and Concrete Research*, 41, 1310–1319.
- Malm, R., & Sundquist, H. (2010). Time-dependent analyses of segmentally constructed balanced cantilever bridges. *Engineering Structures*, 32, 1038–1045.
- MC 10. (2010). *CEB-FIP model code 2010* (6th ed.). London: Thomas Telford.
- MC 90. (1993). *CEB-FIP model code 1990* (6th ed.). London: Thomas Telford.
- Menn, C. (2012). *Prestressed concrete bridges*. Basel: Birkhäuser.
- MIDAS, I. T. C. (1989). Midas Civil.
- Mueller, T. (1969). Alteration of the Highway Bridge over the Aare River in Aarwangen (Umbau der Strassenbruecke ueber die Aare in Aarwangen). *Schweizerische Bauzeitung*, 87(11), 199–203. **(In German)**.
- Müller, H. S., Bažant, Z. P., & Küttner, C. H. (1999). *Data base on creep and shrinkage tests, RILEM Subcommittee 5 report RILEM TC 107-CSP*. Paris: RILEM.
- Müller, H. S., & Hilsdorf, H. K. (1990). Evaluation of the time-dependent behavior of concrete. CEB-Bulletin d'Information, N. 199.
- Neulicheid, A., Obholzer, A., & Carlini, G. (2008). Innalzamento, risanamento e rinforzo del ponte sul rio Sinigo. *Strade e Autostrade*, 70(12). (In Italian)
- Pimanmas, A. (2007). The effect of long-term creep and prestressing on moment redistribution of balanced cantilever cast-in-place segmental bridge. *Journal of Science Technology*, 29(1), 205–216.
- Rüsch, H., Jungwirth, D., & Hilsdorf, H. (1973). Kritische Sichtung der Verfahren zur ... der Einflüsse von Kriechen. *Beton- und Stahlbetonbau* 68(3–4–5), 49–60, 76–86, 152–158. **(In German)**.
- Rüsch, H., Jungwirth, D., & Hilsdorf, H. (1983). *Creep and shrinkage—their effect on the behaviour of concrete structures*. New York: Springer.
- Siviero, E., Briseghella, B., & Zordan, T. (2006). Advanced retrofitting techniques with hybrid use of carbon fibre and external post-tensioning: a case study. In *4th international conference on current and future trends in bridge design, construction and maintenance, Kuala Lumpur, Malaysia*. pp. 215–224.
- Svoboda, A., Klusáček, L., & Olšák, M. (2019). Strengthening and rehabilitation of U-shaped RC Bridges Using Substitute Cable Ducts. *Advances in Materials Science and Engineering*. <https://doi.org/10.1155/2019/8920718>.
- Voigt, W. (1890). Über die innere Reibung der festen Körper. *Abhandlungen der Königlichen Gesellschaft von Wissenschaften zu Göttingen*, 36, 3–47. **(In German)**.
- Vokunnaya, S. S., & Tanaji, T. (2017). Construction stage analysis of segmental cantilever bridge. *International Journal of Civil Engineering and Technology (IJCIET)*, 8(2), 373–382.
- Wagner, O. (1958). *Das Kriechen unbewehrten Betons*. Ernst, Berlin: Deutscher Ausschuss für Stahlbeton. **(In German)**.
- Wagner, O. (1962). *Das Kriechen unbewehrten Betons*. Ernst, Berlin: Deutscher Ausschuss für Stahlbeton. **(In German)**.
- Whitney, C. S. (1932). Plain and reinforced concrete arches. *ACI-Journal*, 28, 479–519.
- Xue, J., Lavorato, D., Bergami, A. V., Nuti, C., Briseghella, B., Marano, G. C., et al. (2018). Severely damaged reinforced concrete circular columns repaired by turned steel rebar and high-performance concrete jacketing with steel or polymer fibers. *Applied Sciences*, 8(9), 1671.

Publisher's Note

Springer Nature remains neutral with regard to jurisdictional claims in published maps and institutional affiliations.